Design and Analysis of Quasi-Integrated Horn Antennas for Millimeter and Submillimeter-Wave Applications

George V. Eleftheriades and Gabriel M. Rebeiz, *Member, IEEE*

***Abstract*—The purpose of this paper is to present a systematic process for the design of multimode quasi-integrated horn antennas, and to provide a full range of practical antenna designs for mullimeter and submillimeter-wave applications. The design methodology is based on the Gaussian beam approach and the structures are optimized for achieving maximum fundamental Gaussian coupling efficiency. For this purpose, a hybrid technique is employed in which the integrated part of the antennas is treated using full-wave analysis, whereas the machined part is treated using an approximate model. This results in a simple and efficient design process. The developed design procedure has been applied for the design of a 20-, 23-, and 25-dB quasi-integrated horn antennas, all with a Gaussian coupling efficiency exceeding 97%. The designed antennas have been tested and characterized using both full-wave analysis and 91/370GHz measurements. The quasi-integrated horn antennas are also examined as feed elements for Cassegrain antenna systems and are proven to be comparable to the traditional machined corrugated horn feeds.**

I. Introduction

THE INTEGRATED-CIRCUIT horn antenna was introduced in [1] and analyzed using a full-wave analysis technique in [2]. It consists of a dipole (or monopole) feed evaporated on a thin dielectric membrane which is suspended in a pyramidal cavity etched in silicon or GaAs. Recently, this antenna has been used in several millimeter and submillimeter-wave applications including a double-polarized antenna design at 93 GHz [4], a 256 element imaging array at 802 GHz [5], and a monopulse tracking system at 94 GHz [6]. However, the wide flare-angle of the integrated-circuit horn antenna, which is dictated by the anisotropic etching involved in its fabrication (70° in silicon), limits its useful aperture size to 1.6 λ and its gain to 13 dB. To this end the quasi-integrated horn antenna was introduced [3], which consists of a machined small flare-angle pyramidal section attached to the integrated portion (Fig. 1). The resulting structure is a simple multimode pyramidal horn with circularly symmetric patterns and low cross-polarization, which is particularly attractive for submillimeter quasi-optical receiver applications. The minimum machined dimension involved in its geometry is around 1.5 λ which enables its fabrication to frequencies up to 2 THz. The purpose of this paper is to describe a systematic approach towards the design of these horn antennas, and to provide a full range of practical quasi-integrated horn antenna designs along with their detailed radiation characteristics. Since a very desirable property of antennas intended for use in quasi-optical systems is the high Gaussian content of their radiated fields [7], the developed design methodology is based on the optimization of the quasi-integrated horns for achieving maximum fundamental Gaussian coupling efficiency. The Gaussian coupling efficiency is particularly important in quasi-optical receiver applications because it directly influences the total system performance with a pronounced effect on the receiver noise temperature [8]. The "Gaussian-beam" approach, proposed here towards the design of multimode horns with symmetric patterns utilizes the aperture fields directly and determines the excitation level of each mode in a simple fashion, unlike traditional methods which require cumbersome manipulations of the far-field radiation patterns [12]–[16]. Also, the large difference between the flare angles of the integrated and the machined parts of the quasi-integrated horn antenna enables the treatment of these two portions independently, resulting in a simple and efficient design process. Specifically, the short and wide flare-angle integrated portion is treated using full-wave analysis whereas the long but gradually flared machined section is analyzed using an approximate model.

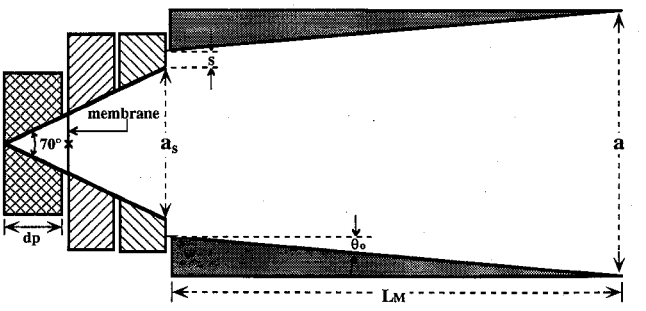

Fig. 1. The general configuration of the quasi-integrated multimode horn antenna.

An outline of the work presented in this paper is as follows. In Section II, a radiating aperture (both with and without phase error) is analyzed for providing maximum coupling efficiency to a fundamental Gaussian beam, and the corresponding necessary conditions for the aperture modes

Manuscript received March 16, 1992; revised September 4, 1992. This work was supported by NASA/Center for Space Terahertz Technology at the University of Michigan.

The authors are with NASA/Center for Space Terahertz Technology, Electrical Engineering and Computer Science Department, University of Michigan, Ann Arbor, MI 48109-2122.

IEEE Log Number 9207407.

are derived. In Section III the optimum aperture fields are examined as feeds to a Cassegrain reflector. The approximate technique for the analysis of the machined section is presented in Section IV along with the description of the design procedure. Subsequently, in Section V, specific quasi-integrated horn designs are considered and verified both numerically using a full-wave analysis technique and experimentally at 91 GHz and 370 GHz.

II. Multimode Aperture Analysis for Maximum Fundamental Gaussian Coupling Efficiency

Consider a square aperture of side a in a ground-plane which is radiating in the half-space $z > 0$. The transverse electric field of the aperture at $z = 0$ can be expanded in terms of the modes of a square waveguide of the same side a:

$$\overline{E}_{t,ap}(x,y) = \sum_{m,n}^{M,N} \{A_{mn}\overline{e}^{\mathrm{TE}}_{mn}(x,y) + C_{mn}\overline{e}^{\mathrm{TM}}_{mn}(x,y)\}, \quad C_{m0} = 0. \tag{1}$$

The TE/TM waveguide modes $\overline{e}^{\mathrm{TE}}_{mn}, \overline{e}^{\mathrm{TM}}_{mn}$ are considered orthonormalized according to:

$$\langle \overline{e}_{mn}, \overline{e}_{pq} \rangle = \iint_{\text{apert}} \overline{e}_{mn}(x,y) \cdot \overline{e}_{pq}(x,y)\, dx\, dy = \delta_{mp}\delta_{nq}. \tag{2}$$

In (1), it is assumed that only modes with subscripts ($m = 1,3,5\cdots M$ and $n = 0,2,4,6\cdots N$) are present as is the case of a pyramidal horn which is either fed by a centered Hertzian dipole or by a waveguide which supports only the dominant TE_{10} mode [2]. We now proceed to determine the modal coefficients A_{mn}, B_{mn} so that the coupling between the aperture field and a fundamental Gaussian beam is maximized. If the copolarized and cross-polarized components of the aperture field are defined to be the $E_{x,ap}$, and the $E_{y,ap}$ components respectively, then the transverse electric field can be rewritten in the form:

$$E_{y,ap}(x,y) = \sum_{m,n}^{M,N} d^{co}_{mn}\Psi^{co}_{mn}(x,y),$$
$$E_{x,ap}(x,y) = \sum_{m,n}^{M,N} d^{xp}_{mn}\Psi^{xp}_{mn}(x,y) \tag{3}$$

where the orthonormalized copolarized and cross-polarized hybrid modes $\Psi^{co}_{mn}, \Psi^{xp}_{mn}$ are defined by

$$\Psi^{co}_{mn}(x,y) = \begin{cases} \dfrac{\sqrt{2\epsilon_n}}{a}(-1)^{\frac{m+n-1}{2}} \cdot \cos\left(\dfrac{m\pi x}{a}\right)\cos\left(\dfrac{n\pi y}{a}\right) \\ \quad \cdot |x| \le a/2, |y| \le a/2 \\ 0, \quad \text{otherwise.} \end{cases} \tag{4}$$

$$\Psi^{xp}_{mn}(x,y) = \begin{cases} \dfrac{\sqrt{2\epsilon_n}}{a}(-1)^{\frac{m+n-1}{2}} \cdot \sin\left(\dfrac{m\pi x}{a}\right)\sin\left(\dfrac{n\pi y}{a}\right) \\ \quad \cdot |x| \le a/2, |y| \le a/2 \\ 0, \quad \text{otherwise.} \end{cases} \tag{5}$$

In (4) and (5) the origin of the Cartesian coordinates is located at the geometrical center of the aperture and $\epsilon_n = 2 - \delta_{n0}$ is the Neumann number. The corresponding copolarized and cross-polarized modal coefficients of (3) are related to the TE/TM modal coefficients of (1) through:

$$d^{co}_{mn} = \frac{nC_{mn} - mA_{mn}}{\sqrt{m^2+n^2}},$$
$$d^{xp}_{mn} = \frac{nA_{mn} + mC_{mn}}{\sqrt{m^2+n^2}}. \tag{6}$$

Now the coupling efficient $\eta(w_o)$ of the aperture to a fundamental Gaussian beam of waist radius w_o, which has its waist on the aperture is calculated to be [17], [18]:

$$\eta(w_o) = \frac{\left|\sum_{m,n}^{M,N} d^{co}_{mn} I_{mn}(w_o)\right|^2}{\frac{w_o^2\pi}{2}\sum_{m,n}^{M,N}(|d^{cp}_{mn}|^2 + |d^{xp}_{mn}|^2)} \tag{7}$$

where

$$I_{mn}(w_o) = \iint_{\text{apert}} \cdot \Psi^{co}_{mn}(x,y)\, \exp\left(-(x^2+y^2)/w_o^2\right) dx\, dy. \tag{8}$$

We wish at this point to determine the modal coefficients d^{co}_{mn} and d^{xp}_{mn} so that the coupling efficiency $\eta(w_o)$ is maximized. For this purpose, the application of Schwarz's inequality to (7) immediately implies that the maximum coupling efficiency $\eta_{\max}(w_o)$ in the presence of cross-polarization is obtained from:

$$\eta_{\max}(w_o) = \frac{\sum_{m,n}^{M,N}|I_{mn}(w_o)|^2}{\frac{w_o^2\pi}{2}} \cdot \frac{\sum_{m,n}^{M,N}|d^{co}_{mn}|^2}{\sum_{m,n}^{M,N}(|d^{cp}_{mn}|^2 + |d^{xp}_{mn}|^2)} \tag{9}$$

with the corresponding copolarization modal coefficients determined by:

$$\frac{d^{co}_{mn}}{I_{mn}(w_o)} = \text{constant}. \tag{10}$$

Condition (10) is recognized to be the condition required for approximating (in the mean square sense) a fundamental Gaussian beam in terms of the aperture modes Ψ^{co}_{mn}. Furthermore, when the cross-polarization vanishes the best maximum coupling efficiency is achieved and is given by:

$$\eta_{\max}(w_o) = \frac{\sum_{m,n}^{M,N}|I_{mn}(w_o)|^2}{\frac{w_o^2\pi}{2}} \tag{11}$$

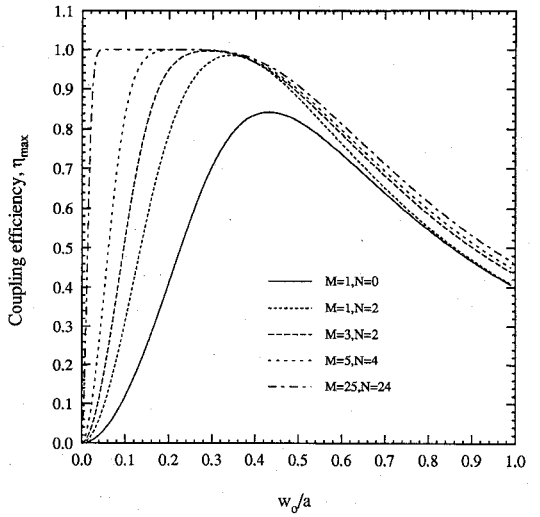

Fig. 2. The maximum Gaussian coupling efficiency as a function of w_o/a ratio when modes up to ($TE_{M,N}/TM_{M,N}, m = 1, 3 \cdots M, n = 0, 2 \cdots N$) are available for beam-shaping on a radiating square aperture of size a which is assumed embedded in an infinite ground plane.

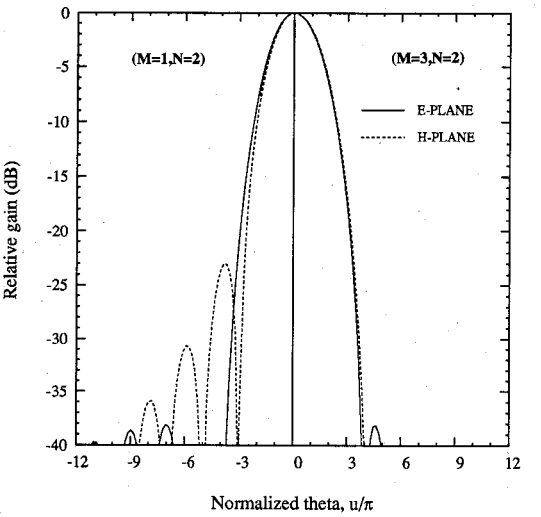

Fig. 3. Universal E and H patterns for the cases ($M = 1, N = 2$) (left), and ($M = 3, N = 2$) (right), $u = (2\pi/\lambda)a \sin(\theta)$. In the H-plane, the paraxial approximation is assumed i.e. $\cos(\theta) \approx 1$ in the main beam.

TABLE I
OPTIMUM PARAMETERS FOR MAXIMUM FUNDAMENTAL GAUSSIAN COUPLING EFFICIENCY FOR CERTAIN PRACTICALLY ENCOUNTERED APERTURE MODES AVAILABLE FOR BEAMSHAPING (UP TO TE_{MN}/TM_{MN})

Available modes (M,N)	(1,0)	(1,2)	(1,2)+TE_{30}	(3,2)
$w_{o,opt}/a$	0.43	0.34	0.32	0.29
cpl. efficiency : η_{max}	84%	98.5%	99.2%	99.7%
$-d_{12}^{co}/d_{10}$	-	0.51	0.56	0.64
$-d_{30}^{co}/d_{10}$	-	-	0.11	0.17
$-d_{32}^{co}/d_{10}$	-	-	-	-0.11

in which case the corresponding condition on the modal coefficients is:

$$nA_{mn} = -mC_{mn}. \tag{12}$$

The maximum coupling efficiency $\eta_{\max}(w_o)$ of (11) still depends on the waist radius w_o and it is shown in Fig. 2 as a function of the ratio w_o/a for various indices (M, N). Some interesting features of this graph are discussed below from the point of view of using the aperture modes to synthesize a certain fundamental Gaussian

1. For each pair of indices (M, N) there exists a corresponding optimum ratio $w_{o,\mathrm{opt}}/a$ for which the coupling efficient attains a global maximum.
2. Large values of w_o/a result in poor coupling efficiencies since most of the synthesized Gaussian power spreads outside the aperture where the aperture electric field vanishes.
3. For a large number of modes available for beamshaping on the aperture, any fundamental Gaussian mode satisfying $w_o/a \leq 0.34$ can be synthesized with corresponding coupling efficiencies approaching 100%. A 100% coupling efficiency is not possible because the synthesized Gaussian beam is always truncated.

In Table I we show the optimum relative magnitudes between the modes as computed numerically from (8) and (10), along with the corresponding optimum $w_{o,\mathrm{opt}}/a$ ratio, for some practically encountered aperture sets of modes. In Fig. 3 we also show the calculated universal far-field E and H patterns for the two cases $(M = 1, N = 2), (M = 3, N = 2)$ and when the aperture modes are excited according to Table I. It is interesting to point out that for the case $(M = 1, N = 2)$, the corresponding ratio of the coefficient of the copolarized hybrid mode given by $\cos(\pi x/a)\cos(2\pi y/a)$ to the dominant mode, given by $\cos(\pi x/a)$, is found to be $\sqrt{2}d_{12}^{co}/d_{10} = 0.72$. This ratio is a compromise between the value of 0.66 required for equalization of the 10 dB beamwidth in the E and H far-field planes and the value of 0.84 required for the cancellation of the E-plane sidelobe [13]. This "far-field" approach of determining the excitation levels of the aperture modes requires the computation of the Fourier transforms of the aperture fields, in contrast to the Gaussian beam approach which directly utilizes the aperture fields. Furthermore, the application of the above far-field design criteria for achieving symmetric patterns becomes cumbersome as the number of aperture modes increases, unlike the Gaussian beam approach which determines the excitation level of every available mode through the simple condition of (10).

The above analysis is valid exactly provided that there is no phase error on the radiating aperture. However, if the aperture is excited by a horn-taper then spherical phase error is introduced which can be approximated by a quadratic wavefront $Q_R(x, y)$ of curvature R (i.e., $Q_R(x, y) = \exp(-(j\pi/\lambda_R)(x^2 + y^2))$. The consequences of this phase error to the performance of dual-mode horns has been studied by Profera [19] who showed that the general effect is the deterioration of the circular symmetry of the patterns and the increase of the sidelobe-level. The Gaussian beam analysis presented above can be extended in a straightforward manner to the case of a nonzero phase error and thus it can still provide design conditions for the aperture modes. In this case, the optimum fundamental Gaussian beam must have its beam waist located at a distance Z_{ap} behind the aperture and inside the horn so that its aperture radius of curvature (R_G) equals the radius of curvature of the aperture field (R) (see Fig. 4). In

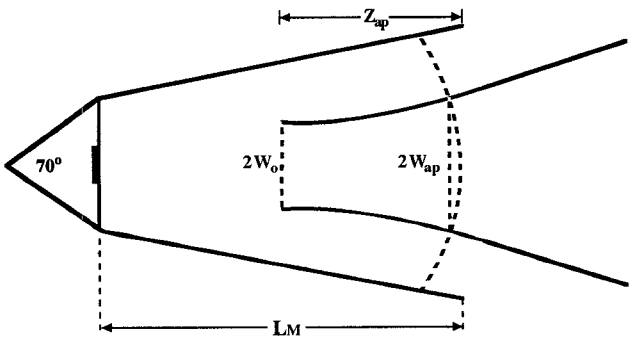

Fig. 4. The definition of the waist radius w_o and the aperture beam radius w_{ap} for the matched Gaussian beam. The beam waist is located at a distance Z_{ap} behind the radiating aperture of the quasi-integrated horn antenna.

the presence of phase error, the copolarized component of the aperture electric field is assumed to be represented in the form:

$$E_{y,ap}(x,y) = Q_R(x,y) \cdot \sum_{m,n}^{M,N} \acute{d}^{co}_{mn} \Psi^{co}_{mn}(x,y). \tag{13}$$

The corresponding coupling efficiency to a fundamental Gaussian mode of aperture beam radius w_{ap} and of aperture radius of curvature R_G is given by [18]:

$$\eta(w_{ap}) = \frac{\left| \iint_{aperture} e^{jk(x^2+y^2)/2R_G} e^{-(x^2+y^2)/w_{ap}^2} E_{y,ap}(x,y)\, dx\, dy \right|^2}{\frac{\pi w_{ap}^2}{2} \iint_{aperture} |\overline{E}_{ap}(x,y)|^2\, dx\, dy}. \tag{14}$$

If now in (14) we choose the aperture field radius of curvature to equal the Gaussian beam radius of curvature, then the quadratic phase factors are eliminated and the corresponding Gaussian coupling efficiency retains the form of (7). However, in this case the beam waist radius w_o should be replaced by the aperture beam radius w_{ap} (Fig. 4) and the copolarized field expansion coefficients d^{co}_{mn} should be replaced by the quadratically phase-modulated coefficients $\acute{d}^{co}_{mn}$. Therefore, the conditions on the coefficients $\acute{d}^{co}_{mn}$ for maximum coupling efficiency are still governed by (10), (12) and the corresponding Gaussian coupling efficiency is still given by (11).

III. Coupling to a Cassegrain Antenna

In this section the multimode horns of Table I are examined as feed elements for Cassegrain reflectors comprising typical submillimeter quasi-optical antenna systems. For a distributed object, the pertinent coupling efficiency of the Cassegrain antenna system is the Gaussian coupling efficiency. Therefore, the optimum coupling efficiency of the Cassegrain system coincides with the optimum coupling efficiencies of the feed elements as tabulated in Table I.

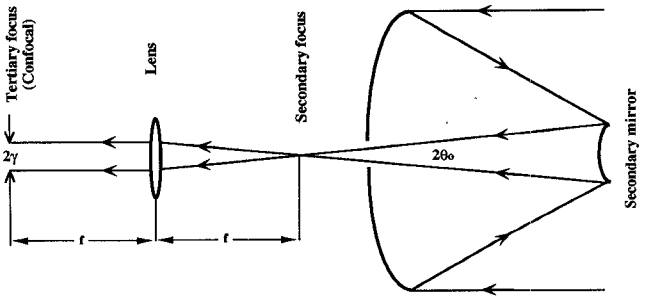

Fig. 5. A Cassegrain antenna system and the associated ray-optics.

In order to complete the efficiency analysis to a Cassegrain antenna system, we also investigate the case for which the object is a point source at infinity. In this case, the pertinent coupling efficiency of the system becomes the coupling to a plane wave. For a long focal-length Cassegrain reflector, the image of a point source at infinity can be accurately represented by the corresponding Airy intensity pattern $J_1(k\rho \sin\theta_o)/(k\rho \sin\theta_o)$, where θ_o is the semi-angle subtended by the subreflector on the secondary focal plane, and ρ is the distance from the reflector axis [9], [10] (see Fig. 5). If a horn-feed having an aperture field distribution $\overline{E}_{ap}(x,y)$ is placed on the secondary focus, the corresponding coupling efficiency can be directly computed from the normalized overlapping integral with the Airy function:

$$\eta_{sec.} = \frac{\left| \iint_{horn\ apert.} \frac{J_1(k\rho \sin\theta_o)}{(k\rho \sin\theta_o)} E_{co}(x,y)\, dx\, dy \right|^2}{\int_{-\infty}^{\infty}\int_{-\infty}^{\infty} \left| \frac{J_1(k\rho \sin\theta_o)}{(k\rho \sin\theta_o)} \right|^2 dx\, dy \iint_{horn\ apert.} |\overline{E}_{ap}(x,y)|^2 dx\, dy} \tag{15}$$

where $E_{co}(x,y)$ is the copolarized component of the aperture field. For a given horn-aperture distribution, the semi-angle θ_o should be selected for maximum coupling efficiency. At this point, we will also examine the coupling to the confocal tertiary focus, which can be computed by transferring the Airy pattern from the secondary to the tertiary focus (see Fig. 5). Since the lens configuration is confocal, and assuming a thin lens of infinite extend and of focal length f, on the tertiary focal plane the Fourier transform of the Airy pattern is formed, which is a uniform circular distribution of radius $\gamma = f \sin\theta_o$. Hence, on the tertiary focus the coupling efficiency becomes:

$$\eta_{ter.} = \frac{\left| \iint_{disc\ \pi\gamma^2} E_{co,ap}(x,y)\, dx\, dy \right|^2}{\pi\gamma^2 \iint_{horn\ apert.} |\overline{E}_{ap}(x,y)|^2\, dx\, dy}. \tag{16}$$

The coupling efficiency expressions of equations (15) and (16) have been employed to construct Table II in which

TABLE II
THE COUPLING EFFICIENCIES ON THE SECONDARY AND C ONFOCAL TERTIARY FOCI OF A CASSEGRAIN ANTENNA FOR THE MULTIMODE FEEDS OF TABLE I, FOR A DIFFRACTION LIMITED CONICAL CORRUGATED HORN OF RADIUS $\rho = a/2$, AND FOR A GAUSSIAN-BEAM FEED OF WAIST RADIUS w_o.

Type of feed	Optimum ($\sin\theta_o$) for coupling to Sec. focus	Cpl. Efficien. on Secondary foc.	Cpl. Efficien. on Tertiary foc.
Conical Corrugated, ρ = a/2	$\frac{1.16}{a/\lambda}$	83.7%	86.9%
Gaussian beam, $\theta_{8.7dB} = \lambda/\pi w_o$	$\frac{1.12}{\theta_{8.7dB}}$	81.5%	81.5%
Multimode up to (1,2)	$\frac{1.08}{a/\lambda}$	83.0%	83.6%
Multimode up to (1,2)+TE_{30}	$\frac{1.15}{a/\lambda}$	83.4%	83.8%
Multimode up to (3,2)	$\frac{1.25}{a/\lambda}$	82.8%	82.9%

TABLE III
DECOMPOSITION OF THE APERTURE FIELDS OF THE MULTIMODE FEEDS, OF THE AIRY PATTERN, AND OF A DIFFRACTION LIMITED CORRUGATED HORN INTO THE FIRST FEW GAUSS-HERMITE MODES

Mode G_{mn}	$J_1(k\rho sin\theta_o)/(k\rho sin\theta_o)$	Up to (1,2)	Up to (1,2)+TE_{30}	Up to (3,2)	Corrug.
0 0	0.9025	0.9925	0.9958	0.9984	0.9903
0 2	0.0	-0.0268	-0.0068	0.0023	0.0
2 0	0.0	0.0238	0.0046	-0.0183	0.0
0 4	-0.1418	-0.0305	-0.0299	-0.0393	-0.0737
4 0	-0.1418	-0.0907	-0.0575	-0.0302	-0.0737
2 2	-0.1158	-0.0006	-0.0377	0.0044	-0.0602
0 6	-0.1028	-0.0048	-0.0041	0.0058	0.0243
6 0	-0.1028	0.0277	-0.0070	-0.0008	0.0243
2 4	-0.0797	-0.0070	-0.0012	0.0019	0.0188
4 2	-0.0797	0.0024	0.0155	-0.0010	0.0188

the optimum coupling efficiencies of the multimode horns of Section II are compared to the optimum efficiencies achieved by a diffraction limited conical corrugated horn of radius a, and by a fundamental Gaussian-beam feed of waist radius w_o. In addition, following Padman [9] we decompose in Table III, the fields of the multimode horns, the field of the diffraction limited corrugated horn, and of the Airy pattern into their first few Gauss-Hermite modal components (for details see the Appendix).

From Table II, it is observed that the multimode horn antennas present 2% higher coupling efficiencies to the Cassegrain reflector than to a pure Gaussian-beam feed, which is due to the presence of higher order Gauss-Hermite modes in their fields (see Table III). The corresponding optimum edge-taper for the multimode horns is found to be around 10.2 dB which is close to the value of 10.9 dB required in the case of a pure Gaussian-beam feed. Furthermore on the tertiary focus, the corrugated horn couples better than the multimode horns. This higher coupling efficiency is achieved because the Fourier transforming action of the lens reverses the phase of the G_{06}, G_{60}, G_{24} and G_{42} Gauss-Hermite modal components of the Airy pattern, enabling a better match to the aperture distribution of the corrugated horn (see Table III and appendix). In order to ensure that the involved modes pass through the lens, so that the higher coupling efficiency is achieved, the lens diameter should be at least six beam radii [9]. In the case of the multimode horns, the component Gauss-Hermite modes are already excited in antiphase as it can be observed from Table III. Therefore, for the multimode horns the effect of the lens on the tertiary focus is not very beneficial to the coupling efficiency of the Cassegrain antenna system.

IV. APPROXIMATE ANALYSIS OF THE MACHINED SECTION AND DESCRIPTION OF THE DESIGN PROCESS

Consider the gradually-flared pyramidal machined section of axial length L_M and of half flare-angle θ_o (see Fig. 1) which is assumed excited at its throat by the ($m = 1, 3, 5 \cdots M$ and $n = 0, 2, 4, 6 \cdots N$) locally propagating waveguide modes. Since the machined section is gradually flared and the incident modes propagating, reflections at the throat are considered negligible and the corresponding transverse electric field is given by:

$$\overline{E}_{t,thr}(x,y) = \sum_{m,n}^{M,N} \{A_{mn}^{th}\overline{e}_{mn}^{th,\mathrm{TE}}(x,y) + C_{mn}^{th}\overline{e}_{mn}^{th,\mathrm{TM}}(x,y)\}. \quad (17)$$

To a first order approximation we can assume that each mode preserves its carried power upon propagating from the throat to the aperture. Also, each mode acquires a phase shift which can be computed by integrating the phase shift contributions from each infinitesimal section of length dz:

$$\Phi_{mn} = \int_0^{L_M} \beta_{mn}(z)\, dz \quad (18)$$

where $\beta_{mn}(z)$ is the local propagation constant of the mnth-mode. The above phase shift has been used extensively for the design of multimode horns [12], [16] and it can be rigorously

justified through a coupled-mode analysis of gradually flared tapers [20]. The aperture field is assumed to be modulated by a quadratic phase factor $Q_{L_T}(x,y)$ of curvature $L_T = a/(2\tan\theta_o)$ with L_T being the total virtual length of the taper. Under the above assumptions and neglecting reflections from the aperture of the tapered section (considered electrically large), the aperture field is simply given by:

$$\overline{E}_{t,ap}(x,y) = Q_{L_T}(x,y) \cdot \sum_{m,n}^{M,N} \{\acute{A}^{ap}_{mn}\overline{e}^{ap,\mathrm{TE}}_{mn}(x,y) + \acute{C}^{ap}_{mn}\overline{e}^{ap,\mathrm{TM}}_{mn}(x,y)\} \quad (19)$$

with the quadratically modulated aperture modal coefficients related to the throat modal coefficients through:

$$\acute{A}^{ap}_{mn} = A^{th}_{mn}\sqrt{Y^{th,\mathrm{TE}}_{mn}/Y_o}\,\exp(-j\Phi_{mn}) \quad (20)$$

$$\acute{C}^{ap}_{mn} = C^{th}_{mn}\sqrt{Y^{th,\mathrm{TM}}_{mn}/Y_o}\,\exp(-j\Phi_{mn}) \quad (21)$$

where Y^{th}_{mn} is the throat admittance for the mnth mode and Y_o is the free-space intrinsic admittance which has been assigned to the aperture modes. Also, the corresponding copolarization and cross-polarization quadratically modulated coefficients $\acute{d}^{co}_{mn}, \acute{d}^{xp}_{mn}$ are still related to $\acute{A}^{ap}_{mn}, \acute{C}^{ap}_{mn}$ through (6). For convenience, from now on these quadratically modulated coefficients will be simply referred to as the radiating aperture modal coefficients. This approximate model can be used for predicting the radiating aperture modal coefficients once the throat modal coefficients have been determined. Note that just for predicting the magnitude of the radiating aperture modal coefficients, knowledge of the machined section length L_M is not required.

In order to optimize the structure of Fig. 1 for achieving maximum coupling efficiency to a fundamental Gaussian beam, the integrated portion aperture size a_s and the mode converting step-size s (see Fig. 1) should be selected so that the magnitudes of the modal coefficients at the radiating aperture (determined by (20) and (21)) satisfy conditions (10) and (12). On the other hand, the length L_M and the flare-angle θ_o of the machined taper should be selected using the phase shift expression (18) to bring the radiating aperture modes in phase. It should be noted here that the 180° phase difference between the TE $_{mn}$-mode and the corresponding TM$_{mn}$-mode required for the cancellation of the cross-polarization (see (12)) should also be provided by the integrated portion and its step-discontinuity. This is because these modes are degenerate and therefore the machined taper cannot change their phase difference. Along those lines a three-stage design process has been established for the quasi-integrated horn antennas and is summarized below:

1. The integrated 70° flare-angle section of the antenna structure of figure 1 (including the step discontinuity) is selected and analyzed independently of the machined section. For this purpose, the dipole-fed integrated portion is assumed to be terminated by an infinite square waveguide of side $(a_s + 2s)$ and is analyzed using the full-wave analysis technique of [2] to obtain the throat modal coefficients A^{th}_{mn}, C^{th}_{mn}. The junction cross-section a_s and the step size s (see Fig. 1) are selected so that the magnitudes of the radiating aperture modal coefficients, as predicted by (20)–(21) and (6), satisfy the optimal conditions (10) and (12) as closely as possible.
2. The infinite waveguide is now replaced by the gradually flared machined section and the assumption is made that the modal coefficients at the throat of the machined section retain their computed values of stage 1. This is a good approximation since the actual excited modal coefficients are determined by the difference between the integrated portion flare-angle and the machined section flare-angle and this difference is always dominated by the large 70° flare-angle of the integrated portion [13]. The length L_M and the flare-angle θ_o of the machined section are then selected iteratively (using 18) so that the modal coefficients $\acute{d}^{co}_{mn}$ appear in phase on the radiating aperture. The shortest possible length is chosen in order to achieve the maximum bandwidth.
3. Finally, the length and the flare-angle of the machined section are "fine-tuned" using the full-wave analysis of [2] for the entire quasi-integrated horn antenna and again for achieving maximum Gaussian coupling efficiency. For this fine-tuning, the coupling efficiency expression of (14) is used and the aperture field is obtained directly from the full-wave analysis. As a general rule, we have found that this fine-tuning only slightly modifies the initially computed parameters L_M and θ_o and therefore its implementation need not be automated.

In Table IV we quantify several practical geometries of integrated portions which have resulted from the first stage of the design process. The optimum aperture coefficients have been determined from (8), (10) and (12) and have already been tabulated in Table I, whereas the magnitudes of the radiating aperture modal coefficients have been predicted from the full-wave analysis of the integrated portion and the approximate model of (20)–(21) for the machined section. This table suggests that necessary condition (10) for achieving maximum fundamental Gaussian coupling efficiency can in practice be closely satisfied, especially with the introduction of a mode converting step-discontinuity. However, the relative modal ratio required for the cancellation of the cross-polarization (12) cannot be satisfactorily generated when maximum Gaussian coupling efficiency criterion (10) is realized. Fortunately, the associated 180° phase shift can exactly be achieved, resulting in non-zero but low cross-polarization of the order of −22 dB in the 45°-plane. In the next section, the integrated section geometries of Table IV are used for the design of particular quasi-integrated horn antennas.

V. Numerical and Experimental Results for Specific Quasi-Integrated Horn Antenna Designs

The algorithm of section IV has been employed for the design of a 20 dB, a 23 dB and a 25 dB quasi-integrated horn antennas, all with a fundamental Gaussian coupling efficiency exceeding 97% and with a full-null beam efficiency of about 99%. These designs provide a complete set of quasi-

TABLE IV
COMPARISON BETWEEN THE OPTIMUM RELATIVE MAGNITUDES OF THE A PERTURE MODES AND THE RELATIVE MAGNITUDES OF THE MODES L AUNCHED AT THE APERTURE BY FOUR PRACTICAL INTEGRATED PORTION SECTIONS. THE EXCITING DIPOLE IS POSITIONED AT A DISTANCE OF 0.39λ FROM THE APEX OF THE HORN. (THE FIRST GEOMETRY EXCITES MODES UP TO THE TE $_{12}$/TM$_{12}$ AND THE PERTINENT OPTIMUM VALUE IS 0.51, WHEREAS THE REST THREE GEOMETRIES EXCITE ALSO THE TE$_{30}$ MODE AND THE PERTINENT VALUE IS 0.56)

	Optimum	$a_s = 1.35\lambda$ $s = 0.0$	$a_s = 1.52\lambda$ $s = 0.0$	$a_s = 1.35\lambda$ $s = 0.17\lambda$	$a_s = 1.57\lambda$ $s = 0.0$
$\lvert\acute{d}_{12}^{co,ap}\rvert/\lvert\acute{d}_{10}^{ap}\rvert$	0.56(0.51*)	0.52	0.50	0.55	0.51
$\lvert\acute{d}_{30}^{ap}\rvert/\lvert\acute{d}_{10}^{ap}\rvert$	0.114	-	0.110	0.117	0.146
$arg(\acute{C}_{12}^{ap}/\acute{A}_{12}^{ap})$	180°	200°	183°	182°	179°
$\lvert\acute{C}_{12}^{ap}\rvert/\lvert\acute{A}_{12}^{ap}\rvert$	2.0	4.5	4.4	5.1	4.3

TABLE V
THE MAIN RADIATION CHARACTERISTICS OF THE 20 dB QUASI-INTEGRATED HORN ANTENNA (SEE TEXT)

	$0.95f_o$	f_o	$1.05f_o$
Gain	19.4dB	20dB	20.6dB
Aperture efficiency	60.6%	62.8%	65.4%
10dB Beamwidth	$37° \pm 1°$	$34° \pm 1.2°$	$32° \pm 1.8°$
Sidelobe-level (E-plane)	−23dB	−27dB	−26.3dB
Cross-pol.(45°)	−22.5dB	−22.7dB	−23dB
Beam-efficiency (to -10dB)	85%	86%	86.5%
Gaussian Coupling	96.4%	97.3%	96.9%
Gaussian Coupling rolloff	95.5%	97.3%	96.5%

integrated horn antennas for applications in the millimeter and submillimeter-wave spectrum. Although in the design process the analysis of the machined section is performed using the approximate method of Section IV, the computation of the radiation characteristics of the finally designed horns is carried out using the full-wave analysis technique of [2]. Furthermore, using this full-wave analysis along with 6 GHz scale-model measurements [3] it was verified that the input impedance of the feeding strip-dipole in the integrated portion of the horn is not affected by the attachment of the machined section. This is due to the fact that the input impedance of the feeding strip-dipole is mainly determined by its local geometrical environment which remains unaffected by the attachment of the machined section. The input impedance for the integrted-circuit horn antennas has already been analyzed theoretically and characterized experimentally in [2] where it was shown that by adjusting the dipole position along the horn axis, the input impedance can be matched to either Schottky or SIS diodes. Therefore, these results which are summarized in [2] are directly applicable to the case of the quasi-integrated horn antennas as well.

For the pattern measurements the antennas were mounted on a two-axis computer-controlled gimbal mount and for source a tunable 85–96 GHz Gunn diode oscillator, modulated at 1 KHz was used. For the 20 dB horn, the signal was video-detected by a beam lead Schottky diode which was soldered to the feeding dipole on the dielectric membrane of the quasi-integrated horn antenna. The corresponding detected signal had a 40 dB S/N ratio and was fed to a PAR-124A lock-in amplifier. For the 23 dB horn, the output of the Gunn oscillator was fed to a 350–370 GHz quadrupler and the signal was detected by a Bismuth microbolometer integrated with the feeding dipole on the dielectric membrane. In this case, the corresponding S/N ratio was 35 dB.

A. 20-dB Quasi-Integrated Horn Antenna

The geometrical parameters for the 20-dB realization were calculated to be ($a_s = 1.35\lambda, 2s = 0.0, L_M = 7\lambda, \theta_o = 9°, dp = 0.39\lambda$) and the numerically computed patterns from the third stage of the design process along with the corresponding 91 GHz measurements have been reported in [3]. In Fig. 6 the principal patterns are compared to the patterns obtained by analyzing the machined section using the approximate method of Section IV. As shown, the approximate model agrees well with both the full-wave analysis and the measurements thus verifying the approximations used in the design process. Figs. 7–10 show the numerically computed vs. the measured patterns at 86.5 GHz and 95.5 GHz, i.e. at the edges of the ±5% bandwidth; As shown, the 10 dB beamwidth does not vary by more than 3° in this frequency range and therefore for the 20 dB horn a pattern bandwidth of about 10% can be defined. The calculated phase center was found to be located at a distance of 1.5λ from the horn aperture for the E-plane and at 1.4λ for the H-plane. The phase center was computed using the standard method of a least-square fit to the residual far-field phase pattern [21]. The phase center was also estimated by fitting an elliptic Gaussian beam having an astigmatic location of its beam waist to the aperture field (see the appendix). Due to the high Gaussian coupling efficiency of the quasi integrated horn the two methods yielded similar results to within a margin of 15%. The rest of the radiation characteristics of this horn at the design frequency and at the edges of the ±5% bandwidth are summarized in Table V. The indicated 10-dB beamwidth fluctuation corresponds to the variation of the beamwidth in an azimuthal far-field cut. The Gaussian coupling efficiency was computed from the full-wave analysis of the entire antenna structure in conjunction with the coupling formula (14). For this purpose the aperture radius of curvature of the Gaussian beam (R_G) was obtained from the expression:

$$R_G = \frac{R_E + R_H}{2} \tag{22}$$

where R_E and R_H are the radii of curvature of the aperture-field in the E-plane and H-plane cuts respectively, as obtained from a least-square fit to the phase of the aperture field. Also, the Gaussian-beam rolloff was calculated at the edges of the ±5% bandwidth using the Gaussian-beam parameters which were calculated at the design frequency f_o.

B. 23-dB Quasi-Integrated Horn Antenna

The optimized design parameters for a 23 dB quasi-integrated horn were found to be ($a_s = 1.52\lambda, 2s = 0.17\lambda, L_M = 13\lambda, \theta_o = 8.5°, dp = 0.39\lambda$) and the computed principal patterns from both the full-wave analysis of the entire antenna and from the approximate model of Section IV are compared in Fig. 11 to corresponding 370 GHz measurements. In Fig. 12 we include also the computed from the full-wave analysis and the measured patterns for the 45°-plane.

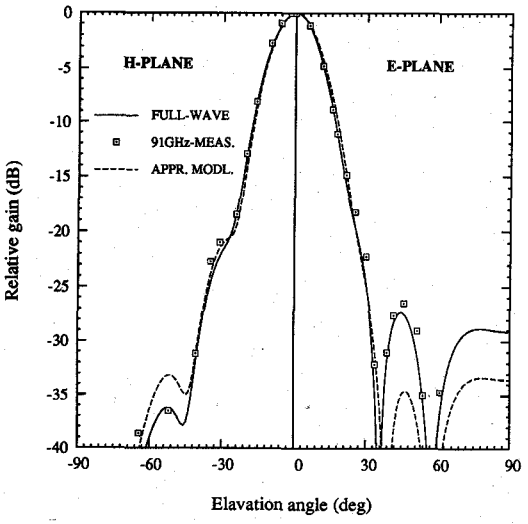

Fig. 6. The E (right) and H-plane (left) patterns of the 20-dB quasi-integrated horn. The 91 GHz measured patterns are compared to the full-wave analysis and the approximate analysis patterns. Detailed patterns including cross-polarization are shown in [3].

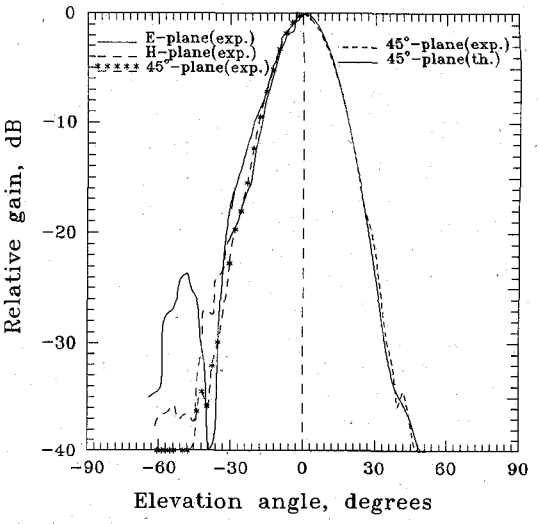

Fig. 8. The measured at 86.5 GHz E/H and 45°-plane patterns vs. the full-wave patterns of the 20-dB quasi-integrated horn.

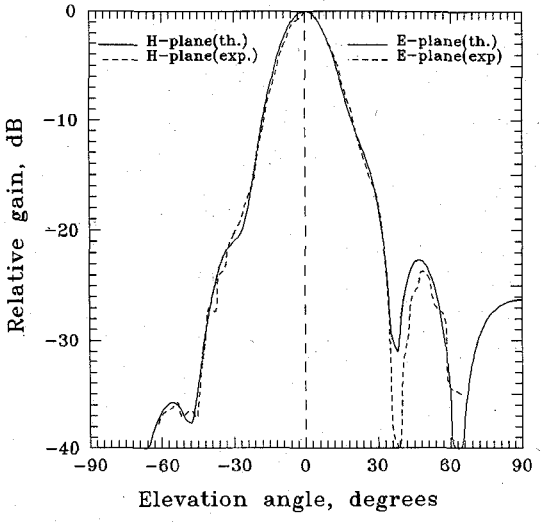

Fig. 7. The measured at 86.5 GHz E (right) and H-plane (left) patterns vs. the full-wave patterns of the 20-dB quasi-integrated horn.

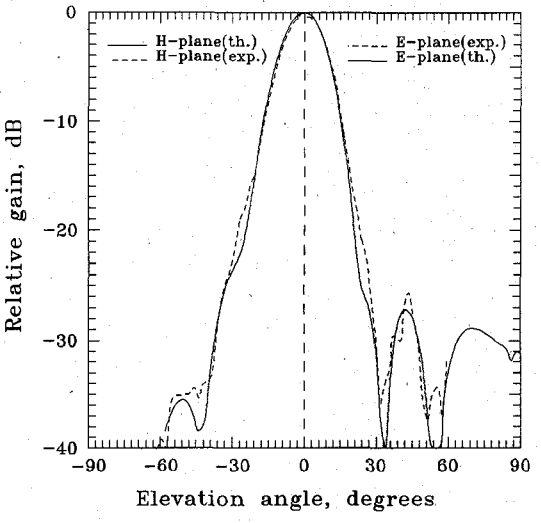

Fig. 9. The measured at 95.5 GHz E (right) and H-plane (left) patterns vs. the full-wave patterns of the 20-dB quasi-integrated horn.

The corresponding E/H and 45°-plane patterns at 358 GHz are shown in Figs. 13 and 14 respectively and the radiation characteristics of this horn are being summarized in Table VI. For the 23 dB horn the phase center was calculated to be at 3.7λ inside the horn for the E-plane and at 3.5λ for the H-plane. Also, the predicted and measured pattern-bandwidth was found to be around 7% when based on the variation of the 10 dB beamwidth. It should be noted here that although the 10 dB beamwidth is sensitive to frequency variations, the symmetry of the patterns and the corresponding Gaussian coupling efficiency are quite insensitive as it can be inferred from Table VI.

C. 25-dB Quasi-Integrated Horn Antenna

In order to evaluate the efficiency of the design process and to provide a full range of practical designs, a 25 dB quasi-integrated horn has also been designed and the computed geometrical parameters were found to be: $(a_s = 1.52\lambda, 2s = 0.0\lambda, L_M = 19.5\lambda, \theta_o = 10°, dp = 0.39\lambda)$. The radiation patterns, as calculated from the full-wave analysis and shown in Fig. 15 still exhibit excellent circular symmetry, low cross-polarization and suppressed sidelobes. The main radiation characteristics of this horn antenna are being tabulated in Table VII. For this longer horn a step discontinuity at the throat of the machined section was avoided in order to provide wider bandwidth. The abrupt change of flare-angle at the throat of the machined section still provides adequate mode conversion as was indicated in Table IV. The corresponding pattern-bandwidth for the 25 dB horn as computed from the change of the 10 dB beamwidth was calculated to be around 7% and the location of the phase center was computed to be at a distance of 13λ from the aperture for the E-plane and at 11λ for the H-plane.

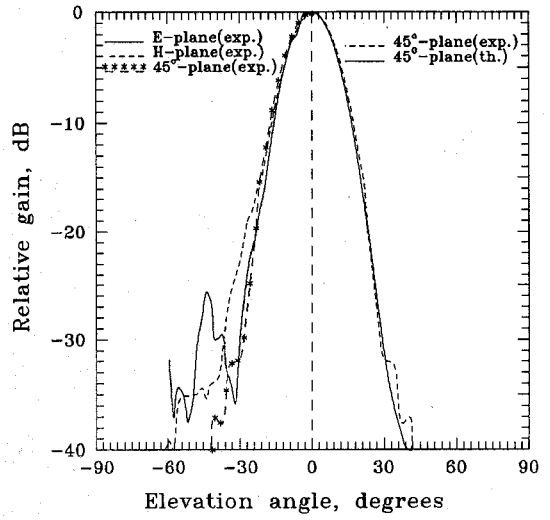

Fig. 10. The measured at 95.5 GHz E/H and 45°-plane patterns vs. the full-wave patterns of the 20-dB quasi-integrated horn.

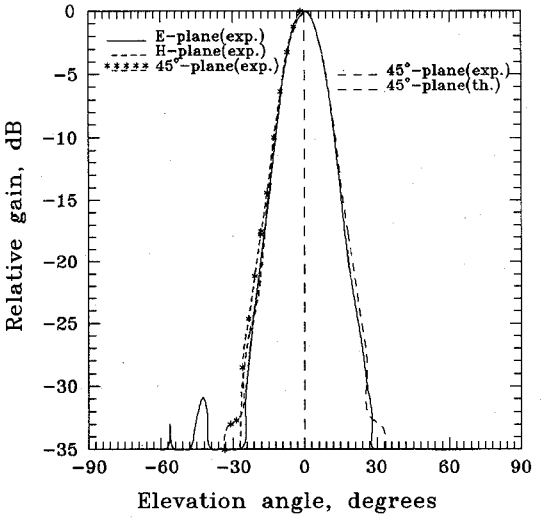

Fig. 12. The measured at 370 GHz E/H and 45°-plane patterns vs. the full-wave patterns of the 23-dB quasi-integrated horn.

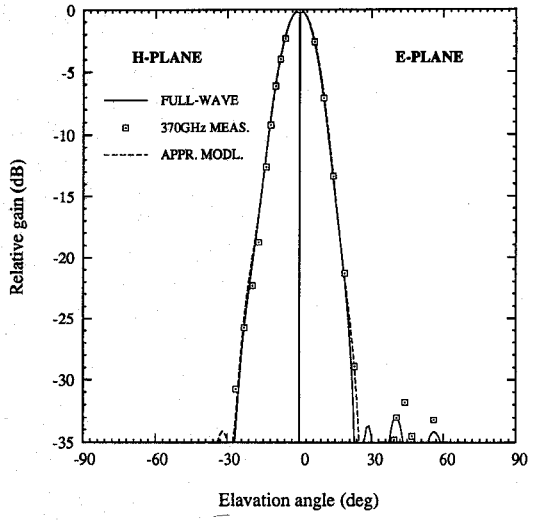

Fig. 11. The E (right) and H-plane (left) patterns of the 23-dB quasi-integrated horn. The 370 GHz measured patterns are compared to the full-wave analysis and the approximate analysis patterns.

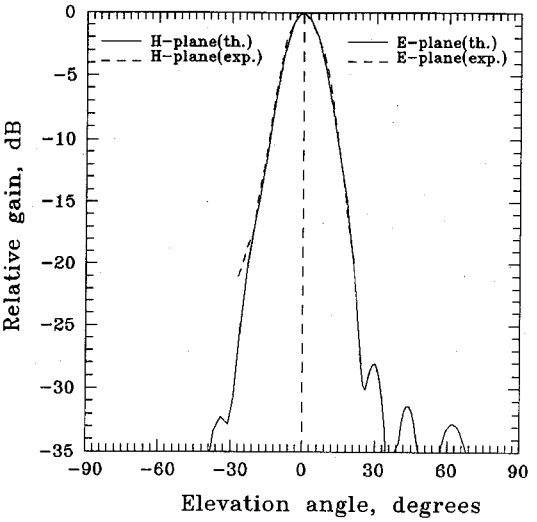

Fig. 13. The measured at 358 GHz E (right) and H-plane (left) patterns vs. the full-wave patterns of the 23-dB quasi-integrated horn.

Below, we discuss some general remarks for all the designed quasi-integrated horn antennas. First, the pattern bandwidth that was used to characterize the frequency sensitivity is quite conservative and depending on the particular application one may choose other criteria to define the bandwidth such as the 10-dB beam efficiency, or the Gaussian coupling efficiency rolloff, in which case the antennas will appear much more wideband. Second, we have found that the phase center of all the antennas considered above is insensitive to frequency variations, at least within the pattern-bandwidth that we have used. Third, the maximum efficiency of a Cassegrain antenna system is obtained when the focus of the antenna coincides with the far-field phase center of the quasi-integrated horns. In this case the computed coupling efficiency (to a plane wave) of the Cassegrain antenna is about 82% for all of the three designed quasi-integrated horns and for both the secondary and the confocal tertiary foci of the Cassegrain antenna. Therefore the use of a confocal lens is unnecessary and is not recommended for the quasi-integrated horn antennas, as has been already pointed out in Section III.

VI. Conclusions

An efficient procedure has been established for the systematic design of quasi-integrated horn antennas for millimeter and submillimeter-wave applications. The design criterion was selected to be the optimization of the structures for maximum fundamental Gaussian coupling efficiency. The implementation of the design method is based on a hybrid technique in which the integrated part of the antennas is analyzed using full-wave analysis whereas the machined gradually flared part is analyzed using an approximate model. The developed design methodology has been employed for the implementation of several quasi-integrated horn antennas with gains ranging from 20 dB–25 dB and with Gaussian coupling efficiencies exceeding 97%. Those antennas have been fabricated and tested successfully at 91 GHz and 370 GHz and they exhibit

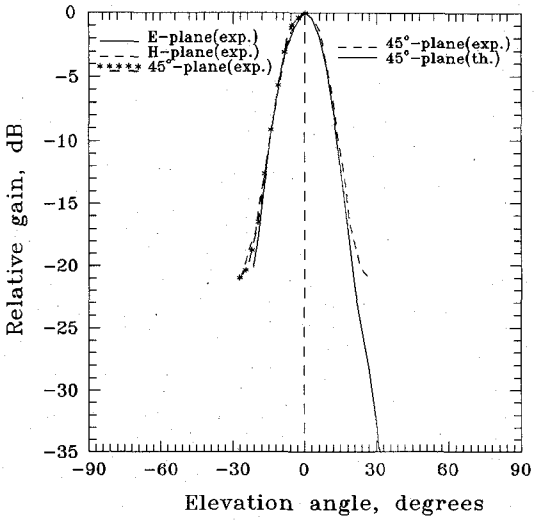

Fig. 14. The measured at 358 GHz GHz E/H and 45°-plane patterns vs. the full-wave patterns of the 23-dB quasi-integrated horn. In this case, the S/N ratio was 23 dB limited by the dynamic range of the lock-in amplifier used.

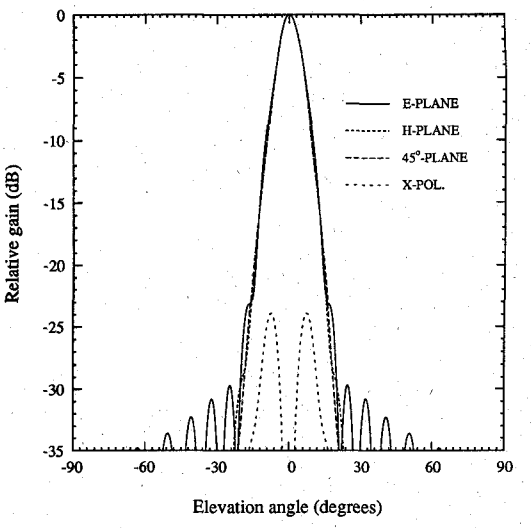

Fig. 15. The calculated from the full-wave analysis patterns of the 25-dB quasi-integrated horn.

TABLE VI
THE MAIN RADIATION CHARACTERISTICS OF THE 23 dB QUASI-I NTEGRATED HORN ANTENNA (S EE TEXT)

	$0.965f_o$	f_o	$1.035f_o$
Gain	22.2dB	22.8dB	23.6dB
Aperture efficiency	48.5%	52%	58.4%
10dB Beamwidth	$27.6 \pm 0.2°$	$25° \pm 1.1°$	$22.5° \pm 1.3°$
Sidelobe-level (E-plane)	−28dB	−33dB	−29.8dB
Cross-pol.(45°)	−20.5dB	−21dB	−22dB
Beam-efficiency (to -10dB)	86.6%	86%	86.6%
Gaussian Coupling	97.2%	97.3%	96.8%
Gaussian Coupling rolloff	96.3%	97.3%	96.0%

TABLE VII
THE MAIN RADIATION CHARACTERISTICS OF THE 25 dB QUASI-I NTEGRATED HORN ANTENNA (SEE TEXT)

	$0.965f_o$	f_o	$1,035f_o$
Gain	24.7dB	25.5dB	26.2dB
Aperture efficiency	36%	40%	44%
10dB Beamwidth	$21.6 \pm 0.8°$	$19.2° \pm 0.7°$	$17.5° \pm 0.5°$
Sidelobe-level (E-plane)	−28.7dB	−30.8dB	−30.8dB
Cross-pol.(45°)	−22.6dB	−24dB	−24.7dB
Beam-efficiency (to -10dB)	84.5%	85%	85%
Gaussian Coupling	97.1%	97.5%	97.4%
Gaussian Coupling rolloff	96.5%	97.5%	97.1%

radiation characteristics which make them very attractive for quasi-optical receiver applications to Terahertz frequencies.

APPENDIX

A. Phase Center Estimation Using a Matched Gaussian Beam

The far-field phase center of the quasi-integrated horns can be estimated from the position of the beam waist of the corresponding matched fundamental Gaussian beam. In principle, higher order Gauss-Hermite modes should be taken into account, but the high fundamental Gaussian content of these antennas guarantee reliable results from only the fundamental Gaussian mode. However, for accurate phase center calculations an elliptic Gaussian beam with an astigmatic location of its E and H plane beam waists should be used. In this case the coupling efficiency of (14) becomes (A1), which is shown at the bottom of this page, where w_E, w_H are the aperture beam-radii in the E and H plane respectively and R_E, R_H are the corresponding radii of curvature of the phase distribution of the aperture field (computed directly from the full-wave analysis). To estimate the phase center, the aperture beam radii w_E and w_H are selected iteratively so that the coupling efficiency η_{el} attains its maximum. The corresponding location of the phase center in the E and the H planes is then obtained from the positions of the beam waists inside the horn Z_E, Z_H, according to:

$$Z_{E,H} = \frac{R_{E,H}}{1 + \left(\dfrac{\lambda R_{E,H}}{\pi w_{E,H}}\right)^2}. \tag{A2}$$

$$\eta_{el} = \frac{\left| \iint\limits_{aperture} e^{jk(x^2/2R_H + y^2/2R_E)} e^{-(x^2/w_H^2 + y^2/W_E^2)} E_{y,ap}(x,y)\, dx\, dy \right|^2}{\dfrac{\pi w_H w_E}{2} \iint\limits_{aperture} |\overline{E}_{ap}(x,y)|^2\, dx\, dy} \tag{A1}$$

Note that for computing the coupling efficiency and in view of the modal expansion of (1), the double integral in the denominator of (A1) is obtained directly from the aperture modal coefficients using Parseval's theorem, whereas the double integral in the numerator is separable and splits into single integrations which are numerically carried out.

B. Expansion of the Fields into Gauss-Hermite Modes

The diffraction limited aperture fields of the multimode antennas of Table I, can be expanded in terms of Gauss-Hermite modes:

$$E_{co}(x,y) = \sum_{m,n} d_{mn} G_{mn}(x,y) \tag{A3}$$

where the orthonormalized Gauss-Hermite modes G_{mn} are given by:

$$G_{mn}(x,y) = \sqrt{\frac{2}{2^m 2^n m! n! \pi w_o^2}} \cdot \exp\left(-\frac{x^2+y^2}{w_o^2}\right) \cdot H_m(\sqrt{2}x/w_o) H_n(\sqrt{2}y/w_o). \tag{A4}$$

In (A4), w_o is the beam waist radius and H_p is the Hermite polynomial of order p. If the expansion coefficients d_{mn} are normalized so that the square of their magnitudes represents the fractional power radiated into the G_{mn} mode, then the normalized coefficients D_{mn} can be defined by:

$$D_{mn} = \frac{d_{mn}}{||E_{co}||} = \frac{\iint_{horn\ apert.} E_{co}(x,y)\, G_{mn}(x,y)\, dx\, dy}{\left(\iint_{horn\ apert.} |E_{co}(x,y)|^2\, dx\, dy\right)^{1/2}}. \tag{A5}$$

In Table III these normalized expansion coefficients are tabulated for the Airy-pattern, for a diffraction limited corrugated horn, and for the multimode fields of Table I. The beam waist radius w_o is chosen in each case so that the fractional power radiated in the fundamental Gauss-Hermite mode G_{00} is maximized. Also, note that if the Airy-pattern normalized expansion coefficients are denoted by D^a_{mn} and the multimode field normalized expansion coefficients are denoted by D^b_{mn} and assuming that the same beam waist radius is used for the expansions, then using the orthonormality of the Gauss-Hermite modes in (15), it is implied that the coupling to the secondary focus of the Cassegrain antenna is given by:

$$\eta_{sec.} = \left|\sum_{m,n} D^a_{mn} D^b_{mn}\right|^2. \tag{A6}$$

Furthermore, upon a Fourier transformation a Gauss-Hermite mode G_{mn} maps within a scale factor into itself and with a sign change determined by i^{m+n}, where i is the square root of -1. This behavior is revealed using the integral [11]:

$$\int_{-\infty}^{\infty} e^{\imath kx} e^{-x^2/2} H_n(x)\, dx = i^n \sqrt{2\pi} e^{-k^2/2} H_n(k). \tag{A7}$$

Therefore, the modes which reverse sign upon a Fourier transformation are those for which $(m+n)/2$ is odd.

ACKNOWLEDGMENT

The authors would like to thank Prof. Linda Katehi for useful discussions. The expertise of Walid Y. Ali-Ahmad in fabricating the antennas and his assistance in carrying out the measurements is gratefully acknowledged.

REFERENCES

[1] G. M. Rebeiz, D. P. Kasilingam, P. A. Stimson, Y. Guo, and D. B. Rutledge, "Monolithic millimeter-wave two-dimensional horn imaging arrays," *IEEE Trans. Antennas Propagat.*, vol. 28, pp. 1473–1482, Sept. 1990.

[2] G. V. Eleftheriades, W. Y. Ali-Ahmad, L. P. B. Katehi, and G. M. Rebeiz, "Millimeter-wave integrated-horn antennas Part I-Theory, and Part II-Experiment," *IEEE Trans. Antennas Propagat.*, vol. 39, pp. 1575–1586, Nov. 1991.

[3] G. V. Eleftheriades, W. Y. Ali-Ahmad, and G. M. Rebeiz, "A 20-dB quasi-integrated horn antenna," *IEEE Microwave Guided Wave Lett.*, vol. 2, pp. 73–75, Feb. 1992.

[4] W. Y. Ali-Ahmad and G. M. Rebeiz, "92 GHz dual-polarized integrated horn antennas," *IEEE Trans. Antennas Propagat.*, vol. 39, pp. 820–825, June 1991.

[5] W. Y. Ali-Ahmad, G. M. Rebeiz, H. Dave, and G. Chin, "802 GHz integrated horn antennas imaging array," *Int. J. Infrared Millimeter Waves*, vol. 12, no. 5, 1991.

[6] C. C. Ling and G. M. Rebeiz, "94 GHz integrated monopulse antenna," *IEEE AP-S Int. Symp.*, ON, Canada, June 1991.

[7] P. F. Goldsmith, "Quasi-optical techniques at millimeter and submillimeter wavelengths," in *Infrared and Millimeter Waves*, vol. 6, New York: Academic, 1982, pp. 243–277.

[8] E. N. Grossman, "The coupling of submillimeter corner-cube antennas to Gaussian beams," *Infrared Phys.*, vol. 29, pp. 875–885, 1989.

[9] R. Padman, J. A. Murphy, and R. E. Hills, "Gaussian mode analysis of Cassegrain antenna efficiency," *IEEE Trans. Antennas Propagat.*, vol. 35, pp. 1093–1103, Oct. 1987.

[10] P. J. B. Clarricoats and A. D. Olver, *Corrugated Horns for Microwave Antennas*. London: Peregrinus (IEE electromagnetic wave series; 18), 1984, pp. 10–19.

[11] I. S. Gradshteyn, I. M. Ryzhik, *Tables of Integrals, Series, and Products*. San Diego, CA: Academic Press, 1980, sixth printing, p. 838.

[12] P. D. Potter, "A new horn antenna with suppressed sidelobes and equal beamwidths," *Microwave J.*, vol. VI, pp. 71–78, June 1963.

[13] S. B. Cohn, "Flare-angle changes in a horn as a means of pattern control," *Microwave J.*, vol. 13, pp. 41–46, Oct. 1970.

[14] P. A. Jensen, "A low-noise multimode Cassegrain monopulse feed with polarization diversity," *Northeast Electron. Res. and Eng. Meeting*, pp. 94–95, Nov. 1963, Copyright 1963 by the Boston Section, IEEE.

[15] A. C. Ludwig, "Radiation pattern synthesis for circular aperture horn antennas," *IEEE Trans. Antennas Propagat.*, vol. AP-14, pp. 434–440, July 1966.

[16] H. M. Pickett, J. C. Hardy, and J. Farhoomand, "Characterization of a dual-mode horn for submillimeter wavelengths," *IEEE Trans. Microwave Theory Tech.*, vol. MTT-32, pp. 936–937, Aug. 1984.

[17] R. J. Wylde, "Millimeter-wave Gaussian beam-mode optics and corrugated feed-horns," *Proc. Inst. Elec. Eng.*, vol. 131, pt. H, no. 4, pp. 258–262, Aug. 1984.

[18] G. V. Eleftheriades and G. M. Rebeiz, "High-gain step-profiled integrated diagonal horn-antennas," *IEEE Trans. Microwave Theory Tech.*, vol. 40, pp. 801–805, May 1992.

[19] C. E. Profera, "Complex radiation patterns of dual mode pyramidal horns," *IEEE Trans. Antennas Propagat.*, vol. AP-25, pp. 436–438, May 1977.

[20] L. Solymar, "Spurious mode generation in nonuniform waveguide," *IRE Trans. Microwave Theory Tech.*, vol. MTT-7, pp. 379–383, 1959.

[21] C. J. Sletten, Ed., *Reflector and Lens Antennas*. Norwood, MA: Artech House, 1981, pp. 89–92.

George V. Eleftheriades was born in Limassol, Cyprus, in May 1963. He received the Diploma in Electrical Engineering with distinction from the National Technical University of Athens, Athens, Greece in 1988 and the M.S. degree in Electrical Engineering from the University of Michigan, Ann Arbor, in December 1989.

Currently he is working towards the Ph.D. degree at the Radiation Laboratory of the University of Michigan. His research interests include millimeter-wave antennas and circuits, Gaussian-beam techniques, phased arrays and analytical techniques in Electromagnetics.

Mr. Eleftheriades received the Best Paper Award at the 1990 International Conference on Antennas, Nice, France and the "Distinguished Achievement Award" from the Electrical Engineering Department of the University of Michigan, in February 1991.

Gabriel M. Rebeiz (S'86–M'88) was born in December 1964 in Beirut, Lebanon. He graduated in 1982 from the American University in Beirut with a B.E. (Honors) in electrical engineering. In September 1982, he joined the California Institute of Technology, and earned the Ph.D. in electrical engineering in June 1988.

He joined the faculty of the University of Michigan in September 1988 where he is now an Assistant Professor in the Electrical Engineering and Computer Science Department.

Dr. Rebeiz has been awarded a NASA-Certificate of Recognition Award for his contribution to the millimeter-wave space program (March 1990) and the Best Paper Award at the 1990 International Conference on Antennas, Nice, France. He received an NSF Presidential Young Investigator Award in 1991. His research interests lie in planar millimeter-wave antennas, receivers and transmitters, and fabrication and measurements of novel millimeter-wave transmission-lines and devices.